A COMPARISON OF TWO FRAMEWORKS FOR KINEMATIC HARDENING IN HYPERELASTO-PLASTICITY

Knut A. Meyer[*], Magnus Ekh

Department of Applied Mechanics, Division of Material and Computational Mechanics,
Chalmers University of Technology, 412 96 Gothenburg, Sweden
e-mail[*]: knut.andreas.meyer@chalmers.se, web page: http://www.chalmers.se/

Key words: Hyperelasto-plasticity, Finite strains, Kinematic hardening

Abstract. In this work we compare two frameworks for thermodynamically consistent hyperelasto-plasticity with kinematic hardening. The first was formulated by Dettmer and Reese (2004), inspired by Lion (2000), and has been used to model sheet metal forming. The second, formulated by Wallin et al. (2003), has been used to model large shear strains and cyclic ratcheting behavior of pearlitic steel (Johansson et al. 2006). In this paper we show that these frameworks can result in equivalent models for certain choices of free energies. Furthermore, it is shown that the choices of free energy found in the literature only result in minor differences. These differences are discussed theoretically and investigated numerically.

1 INTRODUCTION

Large strains in metals during room temperature occur in many technical applications, often during manufacturing, such as sheet metal forming. Some components are also subjected to large strains during service, for example in the surface layer of railway rails and wheels (see e.g. [1, 2]). Experiments have shown that the Bauchinger effect, often modeled with kinematic hardening, is pronounced in many metals. Kinematic hardening can be modeled with different thermodynamically consistent hyperelasto-plastic frameworks found in the literature, and two of them are considered here. The first framework is based on rheological models with an Armstrong-Frederick (AF) type of kinematic hardening, and was proposed by Lion [3] and further developed by Dettmer and Reese [4]. The second framework, introduced by Wallin et al. [5], also features an AF type of kinematic hardening, and has been used to model the Swift effect [6] and large deformations in railway applications [7, 8]. In this paper we compare these frameworks, both theoretically and numerically.

1

2 DESCRIPTION OF FRAMEWORKS

In this section, the modeling frameworks are presented in terms of their assumed kinematics and thermodynamics. The common parts are presented in Subsections 2.1 and 2.2, followed by a description of how the frameworks differ in Subsections 2.3 and 2.4. Three specific models are defined in Subsections 2.5 and 2.6, which are compared in the numerical examples in Section 3. For the clarity of the presentation, only linear kinematic hardening is considered in the current section. In Section 4 we investigate nonlinear kinematic hardening, e.g. of Armstrong-Frederick type.
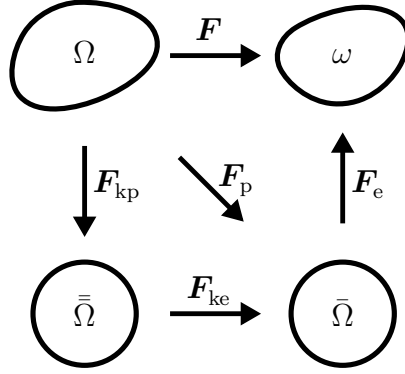

Figure 1: Configurations and deformation gradients

2.1 Kinematics and notations

Figure 1 shows the different configurations used in both [4] and [5]. Dettmer and Reese [4] introduce the inelastic plastic deformation gradient $\boldsymbol{F}_{\text{kp}}$ connecting the fictitious kinematic configuration $\bar{\bar{\Omega}}$ to the initial configuration Ω. This connection is not introduced in Wallin et al. [5], but otherwise the same configurations and remaining deformation gradients are present in both frameworks.

Tensors on the current configuration ω are denoted with lower case letters and no bars, e.g. $\boldsymbol{b}$. Tensors on the intermediate $\bar{\Omega}$ and kinematic $\bar{\bar{\Omega}}$ configurations are denoted by one bar, e.g. $\bar{\boldsymbol{C}}_{\text{e}}$, and two bars, e.g. $\bar{\bar{\boldsymbol{C}}}_{\text{ke}}$, respectively. The following decompositions of the deformation gradients and definitions of the deformation tensors will be used:

$$
\begin{aligned}
\boldsymbol{F} &= \boldsymbol{F}_{\text{e}}\boldsymbol{F}_{\text{p}} & \bar{\boldsymbol{C}}_{\text{e}} &= \boldsymbol{F}_{\text{e}}^{\text{t}}\boldsymbol{F}_{\text{e}} & \boldsymbol{c}_{\text{e}} &= \boldsymbol{F}_{\text{e}}^{-\text{t}}\boldsymbol{F}_{\text{e}}^{-1} = \boldsymbol{b}_{\text{e}}^{-1} \\
\boldsymbol{F}_{\text{p}} &= \boldsymbol{F}_{\text{ke}}\boldsymbol{F}_{\text{kp}} & \bar{\bar{\boldsymbol{C}}}_{\text{ke}} &= \boldsymbol{F}_{\text{ke}}^{\text{t}}\boldsymbol{F}_{\text{ke}} & \bar{\boldsymbol{c}}_{\text{ke}} &= \boldsymbol{F}_{\text{ke}}^{-\text{t}}\boldsymbol{F}_{\text{ke}}^{-1} = \bar{\boldsymbol{b}}_{\text{ke}}^{-1}
\end{aligned}
\tag{1}
$$

The velocity gradients on the intermediate and kinematic configurations are defined as

$$
\bar{\boldsymbol{L}}_{\text{p}} = \dot{\boldsymbol{F}}_{\text{p}}\boldsymbol{F}_{\text{p}}^{-1}
\tag{2}
$$

$$
\bar{\boldsymbol{L}}_{\text{ke}} = \dot{\boldsymbol{F}}_{\text{ke}}\boldsymbol{F}_{\text{ke}}^{-1}
\tag{3}
$$

$$
\bar{\bar{\boldsymbol{L}}}_{\text{kp}} = \dot{\boldsymbol{F}}_{\text{kp}}\boldsymbol{F}_{\text{kp}}^{-1}
\tag{4}
$$

and hence the velocity gradient l on the current configuration can be written as

$$l = \dot{F}F^{-1} = \dot{F}_\mathrm{e}F_\mathrm{e}^{-1} + F_\mathrm{e}\bar{L}_\mathrm{p}F_\mathrm{e}^{-1} \qquad (5)$$

2.2   Thermodynamics

The free energy Ψ is introduced with the additive split according to

$$\Psi = \Psi_\mathrm{e}\left(\bar{C}_\mathrm{e}\right) + \Psi_\mathrm{kin}\left(F_\mathrm{ke}\right) \qquad (6)$$

whereby the dissipation inequality (see e.g. Simo (1998) [9]) becomes

$$D = \boldsymbol{\tau} : l - \dot{\Psi} = \boldsymbol{\tau} : l - \frac{\partial \Psi_\mathrm{e}}{\partial \bar{C}_\mathrm{e}}\dot{\bar{C}}_\mathrm{e} - \frac{\partial \Psi_\mathrm{kin}}{\partial F_\mathrm{ke}} : \dot{F}_\mathrm{ke} \geq 0 \qquad (7)$$

where $\boldsymbol{\tau}$ is the Kirchhoff stress. Using the requirement of zero dissipation during elastic loading and Equation (5), the reduced dissipation inequality becomes

$$D = \bar{M} : \bar{L}_\mathrm{p} - \left(\frac{\partial \Psi_\mathrm{kin}}{\partial F_\mathrm{ke}}F_\mathrm{ke}^\mathrm{t}\right) : \bar{L}_\mathrm{ke} \qquad (8)$$

where the Mandel stress $\bar{M}$ is defined as

$$\bar{M} = 2\bar{C}_\mathrm{e}\frac{\partial \Psi_\mathrm{e}}{\partial \bar{C}_\mathrm{e}} \qquad (9)$$

In a standard fashion, we adopt an associative evolution of the plastic deformation gradient in this paper:

$$\bar{L}_\mathrm{p} = \dot{\lambda}\frac{\partial \Phi}{\partial \bar{M}} \qquad (10)$$

where the functional dependence of the yield function $\Phi \leq 0$ will be specified later. Up until this point the two frameworks are identical. We first describe the framework by Dettmer and Reese [4], before proceeding with the framework by Wallin et al. [5].

2.3   1st framework [4]

In the first framework proposed by Lion [3] and further developed by Dettmer and Reese [4], the plastic deformation gradient F_p is multiplicatively decomposed into an elastic part F_ke and a plastic part F_kp. The physical motivation is that F_ke represents local elastic deformations on the microscale caused by dislocations and F_kp represents irreversible displacements in the slip systems. The assumption is that development of F_ke results in linear kinematic hardening and the development of F_kp reduces F_ke, hence causing saturation (dynamic recovery) of the kinematic hardening. This is illustrated using a rheological model by Lion [3]. The multiplicative split of F_p results in the following additive split of the plastic velocity gradient $\bar{L}_\mathrm{p}$

$$\bar{L}_\mathrm{p} = \bar{L}_\mathrm{ke} + F_\mathrm{ke}\bar{\bar{L}}_\mathrm{kp}F_\mathrm{ke}^{-1} \qquad (11)$$

For the case of purely linear hardening ($\boldsymbol{F}_{\mathrm{kp}} = \boldsymbol{I}$), the reduced dissipation, Equation (8), can be written as

$$D = \left(\bar{\boldsymbol{M}} - {}^1\bar{\boldsymbol{M}}_{\mathrm{k}}\right) : \bar{\boldsymbol{L}}_{\mathrm{p}} \tag{12}$$

where the kinematic hardening stress of Mandel type (also denoted back-stress) is defined as

$$ {}^1\bar{\boldsymbol{M}}_{\mathrm{k}} = \frac{\partial \Psi_{\mathrm{kin}}}{\partial \boldsymbol{F}_{\mathrm{ke}}} \boldsymbol{F}_{\mathrm{ke}}^{\mathrm{t}} \tag{13}$$

This motivates that the driving force for plastic flow is $\bar{\boldsymbol{M}} - {}^1\bar{\boldsymbol{M}}_{\mathrm{k}}$ and thereby a yield criterion expressed as $\Phi(\bar{\boldsymbol{M}} - {}^1\bar{\boldsymbol{M}}_{\mathrm{k}})$.

2.4   2nd framework [5]

In the second framework, proposed by Wallin et al. [5], the deformation gradient $\boldsymbol{F}_{\mathrm{ke}}^{-1}$ is introduced to model the deformation of the crystal lattice, due to the residual micro stresses responsible for the Bauchinger effect. From this deformation gradient the kinematic hardening stress of Mandel type is defined as

$$ {}^2\bar{\boldsymbol{M}}_{\mathrm{k}} = -\frac{\partial \Psi_{\mathrm{kin}}}{\partial \boldsymbol{F}_{\mathrm{ke}}} \boldsymbol{F}_{\mathrm{ke}}^{\mathrm{t}} \tag{14}$$

which yields that the reduced dissipation inequality (8) is

$$D = \bar{\boldsymbol{M}} : \bar{\boldsymbol{L}}_{\mathrm{p}} + {}^2\bar{\boldsymbol{M}}_{\mathrm{k}} : \bar{\boldsymbol{L}}_{\mathrm{ke}} \tag{15}$$

Using the standard interpretation of ${}^2\bar{\boldsymbol{M}}_{\mathrm{k}}$ as a back-stress that reduces the driving force for plasticity, motivates the yield function $\Phi(\bar{\boldsymbol{M}} - {}^2\bar{\boldsymbol{M}}_{\mathrm{k}})$. This gives, by the postulate of maximum dissipation, the kinematic relation

$$\bar{\boldsymbol{L}}_{\mathrm{p}} = -\bar{\boldsymbol{L}}_{\mathrm{ke}} \tag{16}$$

and the same reduced dissipation inequality as in Equation (12) is obtained:

$$D = \left(\bar{\boldsymbol{M}} - {}^2\bar{\boldsymbol{M}}_{\mathrm{k}}\right) : \bar{\boldsymbol{L}}_{\mathrm{p}} \tag{17}$$

2.5   Specific formats for free energy

The elastic and kinematic free energies (with the third invariant $I_{3\bullet} = \det(\bullet)$) proposed by Vladimirov et al [10] are

$$ {}^{\mathrm{A}}\Psi_{\mathrm{e}} = \frac{1}{2} G \left(\mathrm{tr}(\bar{\boldsymbol{C}}_{\mathrm{e}}) - 3 - \ln\left(I_{3\mathrm{C}_{\mathrm{e}}}\right) \right) + \frac{\Lambda}{4} \left(I_{3\mathrm{C}_{\mathrm{e}}} - 1 - \ln\left(I_{3\mathrm{C}_{\mathrm{e}}}\right) \right) \tag{18}$$

$$ {}^{\mathrm{A}}\Psi_{\mathrm{kin}} = \frac{1}{2} H_{\mathrm{kin}} \left(\mathrm{tr}(\bar{\bar{\boldsymbol{C}}}_{\mathrm{ke}}) - 3 - \ln\left(I_{3\mathrm{C}_{\mathrm{ke}}}\right) \right) \tag{19}$$

4

The part of the elastic free energy, corresponding to Lamé's second parameter Λ, is thus not included in the kinematic free energy.

A similar split is introduced in [5], but the free energy in that work is decomposed into an isochoric and a volumetric part. The formulation for the volumetric part is not the same in [5] and [7, 8], and here we use the formulation from [7, 8]. This difference only affects the bulk elastic response and the influence on the numerical results studied in this paper is therefore negligible.

$$^{\mathrm{B}}\Psi_{\mathrm{e}} = \frac{1}{2}G\left(\mathrm{tr}\left(I_{3\mathrm{C_e}}^{-1/3}\bar{\boldsymbol{C}}_{\mathrm{e}}\right) - 3\right) + \frac{1}{2}K\left(I_{3\mathrm{C_e}}^{1/2} - 1\right)^2 \tag{20}$$

$$^{\mathrm{B}}\Psi_{\mathrm{kin}} = \frac{1}{2}H_{\mathrm{kin}}\left(\mathrm{tr}\left(I_{3\mathrm{c_{ke}}}^{-1/3}\bar{\boldsymbol{c}}_{\mathrm{ke}}\right) - 3\right) \tag{21}$$

From the discussion so far, there seem to be several differences between the frameworks: (1) the definition of the Mandel back-stress ($^1\bar{\boldsymbol{M}}_{\mathrm{k}}$ or $^2\bar{\boldsymbol{M}}_{\mathrm{k}}$), (2) the variable of which the kinematic free energy depends on ($\bar{\bar{\boldsymbol{C}}}_{\mathrm{ke}}$ or $\bar{\boldsymbol{c}}_{\mathrm{ke}}$) and (3) what part of the elastic free energy formulation that is used to formulate the kinematic free energy. The third of these can be investigated by taking the format of free energy from the second framework, but using the definitions and variables from the first framework to obtain model C:

$$^{\mathrm{C}}\Psi_{\mathrm{e}} = {}^{\mathrm{B}}\Psi_{\mathrm{e}} \tag{22}$$

$$^{\mathrm{C}}\Psi_{\mathrm{kin}} = \frac{1}{2}H_{\mathrm{kin}}\left(\mathrm{tr}\left(I_{3\mathrm{C_{ke}}}^{-1/3}\bar{\bar{\boldsymbol{C}}}_{\mathrm{ke}}\right) - 3\right) \tag{23}$$

2.6   Stresses for each model

We have now described both frameworks, the first by Dettmer and Reese [4] and the second by Wallin et al. [5]. By letting Ψ_{kin} depend on $\bar{\bar{\boldsymbol{C}}}_{\mathrm{ke}}$ or $\bar{\boldsymbol{c}}_{\mathrm{ke}}$ we can use (13) and (14), respectively, to obtain the Mandel back-stresses for the two frameworks:

$$^1\bar{\boldsymbol{M}}_{\mathrm{k}} = \left(\frac{\partial\Psi_{\mathrm{kin}}}{\partial\bar{\bar{\boldsymbol{C}}}_{\mathrm{ke}}} : \frac{\partial\bar{\bar{\boldsymbol{C}}}_{\mathrm{ke}}}{\partial\boldsymbol{F}_{\mathrm{ke}}}\right)\boldsymbol{F}_{\mathrm{ke}}^{\mathrm{t}} = 2\boldsymbol{F}_{\mathrm{ke}}\left(\frac{\partial\Psi_{\mathrm{kin}}}{\partial\bar{\bar{\boldsymbol{C}}}_{\mathrm{ke}}}\right)\boldsymbol{F}_{\mathrm{ke}}^{\mathrm{t}} \tag{24}$$

$$^2\bar{\boldsymbol{M}}_{\mathrm{k}} = -\left(\frac{\partial\Psi_{\mathrm{kin}}}{\partial\bar{\boldsymbol{c}}_{\mathrm{ke}}} : \frac{\partial\bar{\boldsymbol{c}}_{\mathrm{ke}}}{\partial\boldsymbol{F}_{\mathrm{ke}}}\right)\boldsymbol{F}_{\mathrm{ke}}^{\mathrm{t}} = 2\bar{\boldsymbol{c}}_{\mathrm{ke}}\frac{\partial\Psi_{\mathrm{kin}}}{\partial\bar{\boldsymbol{c}}_{\mathrm{ke}}} \tag{25}$$

The Mandel stresses for model A, $^{\mathrm{A}}\bar{\boldsymbol{M}}$ and $^{\mathrm{A}}\bar{\boldsymbol{M}}_{\mathrm{k}}$, are found using Equations (9) and (24) with the free energies in Equations (18) and (19):

$$^{\mathrm{A}}\bar{\boldsymbol{M}} = G(\bar{\boldsymbol{C}}_{\mathrm{e}} - \boldsymbol{I}) + \frac{\Lambda}{2}(I_{3\mathrm{C_e}} - 1)\boldsymbol{I}, \qquad\qquad {}^{\mathrm{A}}\bar{\boldsymbol{M}}_{\mathrm{k}} = H_{\mathrm{kin}}\left(\bar{\boldsymbol{b}}_{\mathrm{ke}} - \boldsymbol{I}\right) \tag{26}$$

The stresses for model B, $^{\mathrm{B}}\bar{\boldsymbol{M}}$ and $^{\mathrm{B}}\bar{\boldsymbol{M}}_{\mathrm{k}}$, are given by using Equations (9) and (25) with the free energies in Equations (20) and (21):

$$^{\mathrm{B}}\bar{\boldsymbol{M}} = GI_{3\mathrm{C_e}}^{-1/3}\bar{\boldsymbol{C}}_{\mathrm{e}}^{\mathrm{dev}} + K(I_{3\mathrm{C_e}} - I_{3\mathrm{C_e}}^{1/2})\boldsymbol{I}, \qquad\qquad {}^{\mathrm{B}}\bar{\boldsymbol{M}}_{\mathrm{k}} = H_{\mathrm{kin}}I_{3\mathrm{c_{ke}}}^{-1/3}\bar{\boldsymbol{c}}_{\mathrm{ke}}^{\mathrm{dev}} \tag{27}$$

For model C, we use the first framework, i.e. the stresses $^{\mathrm{C}}\bar{\boldsymbol{M}}$ and $^{\mathrm{C}}\bar{\boldsymbol{M}}_{\mathrm{k}}$ are given by using Equations (9) and (24), but with the free energies in Equations (22) and (23). We further note that $I_{3\mathrm{C}_{\mathrm{ke}}} = I_{3\mathrm{b}_{\mathrm{ke}}}$ and $\mathrm{tr}(\bar{\bar{\boldsymbol{C}}}_{\mathrm{ke}}) = \mathrm{tr}(\bar{\boldsymbol{b}}_{\mathrm{ke}})$, which leads to:

$$^{\mathrm{C}}\bar{\boldsymbol{M}} = {}^{\mathrm{B}}\bar{\boldsymbol{M}} \qquad\qquad\qquad {}^{\mathrm{C}}\bar{\boldsymbol{M}}_{\mathrm{k}} = H_{\mathrm{kin}} I_{\mathrm{b}_{\mathrm{ke}}}^{-1/3} \bar{\boldsymbol{b}}_{\mathrm{ke}}^{\mathrm{dev}} \qquad (28)$$

If $^{\mathrm{B}}\bar{\boldsymbol{c}}_{\mathrm{ke}} = {}^{\mathrm{C}}\bar{\boldsymbol{b}}_{\mathrm{ke}}$ then clearly model B and C are equivalent. Assuming that is the case for some point in time, we also have $^{\mathrm{B}}\bar{\boldsymbol{L}}_{\mathrm{p}} = {}^{\mathrm{C}}\bar{\boldsymbol{L}}_{\mathrm{p}} = \bar{\boldsymbol{L}}_{\mathrm{p}}$. Since model B is using the second framework, and model C is using the first, we also have $-{}^{\mathrm{B}}\bar{\boldsymbol{L}}_{\mathrm{ke}} = {}^{\mathrm{C}}\bar{\boldsymbol{L}}_{\mathrm{ke}} = \bar{\boldsymbol{L}}_{\mathrm{p}}$, hence

$$^{\mathrm{B}}\dot{\bar{\boldsymbol{c}}}_{\mathrm{ke}} = -\left({}^{\mathrm{B}}\bar{\boldsymbol{L}}_{\mathrm{ke}}^{\mathrm{t}}\,{}^{\mathrm{B}}\bar{\boldsymbol{c}}_{\mathrm{ke}} + {}^{\mathrm{B}}\bar{\boldsymbol{c}}_{\mathrm{ke}}\,{}^{\mathrm{B}}\bar{\boldsymbol{L}}_{\mathrm{ke}}\right) = \bar{\boldsymbol{L}}_{\mathrm{p}}^{\mathrm{t}}\,{}^{\mathrm{B}}\bar{\boldsymbol{c}}_{\mathrm{ke}} + {}^{\mathrm{B}}\bar{\boldsymbol{c}}_{\mathrm{ke}}\bar{\boldsymbol{L}}_{\mathrm{p}} \qquad (29)$$

$$^{\mathrm{C}}\dot{\bar{\boldsymbol{b}}}_{\mathrm{ke}} = \left({}^{\mathrm{C}}\bar{\boldsymbol{L}}_{\mathrm{ke}}\,{}^{\mathrm{C}}\bar{\boldsymbol{b}}_{\mathrm{ke}} + {}^{\mathrm{C}}\bar{\boldsymbol{b}}_{\mathrm{ke}}\,{}^{\mathrm{C}}\bar{\boldsymbol{L}}_{\mathrm{ke}}^{\mathrm{t}}\right) = \bar{\boldsymbol{L}}_{\mathrm{p}}\,{}^{\mathrm{C}}\bar{\boldsymbol{b}}_{\mathrm{ke}} + {}^{\mathrm{C}}\bar{\boldsymbol{b}}_{\mathrm{ke}}\bar{\boldsymbol{L}}_{\mathrm{p}}^{\mathrm{t}} \qquad (30)$$

As $^{\mathrm{B}}\bar{\boldsymbol{c}}_{\mathrm{ke}} = {}^{\mathrm{C}}\bar{\boldsymbol{b}}_{\mathrm{ke}} = \boldsymbol{I}$ initially, the statement $^{\mathrm{B}}\bar{\boldsymbol{c}}_{\mathrm{ke}} = {}^{\mathrm{C}}\bar{\boldsymbol{b}}_{\mathrm{ke}}$ is true for all points in time under the assumption that $\bar{\boldsymbol{L}}_{\mathrm{p}}$ is symmetric. If the free energy is isotropic, the Mandel stresses $\bar{\boldsymbol{M}}$ and $\bar{\boldsymbol{M}}_{\mathrm{k}}$ are symmetric, and hence $\bar{\boldsymbol{L}}_{\mathrm{p}}$ becomes symmetric for the associative choice of $\bar{\boldsymbol{L}}_{\mathrm{p}}$ in Equation (10). This leads to the conclusion that model B and C are equivalent, which is verified numerically later. Furthermore, this proof leads to the interesting conclusion that the frameworks can give exactly the same model with proper choices of free energy. The possibility to formulate an unsymmetric $\bar{\boldsymbol{L}}_{\mathrm{p}}$ for isotropy is discussed in e.g. Wallin et al. [5] and Wallin and Ristinmaa [6], but is not investigated in this paper.

3 NUMERICAL RESULTS

In this section we evaluate the response of the material models for uniaxial loading and simple shear loading. The models are implemented using a standard Backward Euler integration scheme, for which Vladimirov et al. [10] noted that the accuracy suffers at large time steps. To avoid these accuracy problems, approximately $4 \cdot 10^4$ and $5 \cdot 10^4$ load steps are used for the uniaxial and simple shear loading, respectively.

The von Mises effective stress is used to define the yield function Φ according to

$$\Phi = \sqrt{\frac{3}{2}}\sqrt{\mathrm{dev}\left(\bar{\boldsymbol{M}}^{\mathrm{t}} - \bar{\boldsymbol{M}}_{\mathrm{k}}^{\mathrm{t}}\right) : \mathrm{dev}\left(\bar{\boldsymbol{M}} - \bar{\boldsymbol{M}}_{\mathrm{k}}\right)} - Y_0 = f\left(\bar{\boldsymbol{M}} - \bar{\boldsymbol{M}}_{\mathrm{k}}\right) - Y_0 \leq 0 \qquad (31)$$

whereby the evolution of the plastic deformation gradient in (10) becomes

$$\bar{\boldsymbol{L}}_{\mathrm{p}} = \dot{\lambda}\frac{3}{2}\frac{\mathrm{dev}\left(\bar{\boldsymbol{M}}^{\mathrm{t}} - \bar{\boldsymbol{M}}_{\mathrm{k}}^{\mathrm{t}}\right)}{f\left(\bar{\boldsymbol{M}} - \bar{\boldsymbol{M}}_{\mathrm{k}}\right)} \qquad (32)$$

From this it follows that the plastic deformation is isochoric: By time differentiation of $\det\left(\boldsymbol{F}_{\mathrm{p}}\right)$ and using (2)

$$\frac{\partial}{\partial t}\det\left(\boldsymbol{F}_{\mathrm{p}}\right) = \det\left(\boldsymbol{F}_{\mathrm{p}}\right)\boldsymbol{F}_{\mathrm{p}}^{-\mathrm{t}} : \left(\bar{\boldsymbol{L}}_{\mathrm{p}}\boldsymbol{F}_{\mathrm{p}}\right) = \det\left(\boldsymbol{F}_{\mathrm{p}}\right)\mathrm{tr}\left(\bar{\boldsymbol{L}}_{\mathrm{p}}\right) = 0 \qquad (33)$$

hence, $\det\left(\boldsymbol{F}_{\mathrm{p}}\right) = 1$.

The following material parameters: $G = 81\,\mathrm{GPa}$, $K = 174\,\mathrm{GPa}$, $\Lambda = K - 2G/3$, $Y_0 = 100\,\mathrm{MPa}$ and $H_{\mathrm{kin}} = 1000\,\mathrm{MPa}$, are used in the numerical examples in Figure 2.

(a) Uniaxial response   (b) Simple shear response
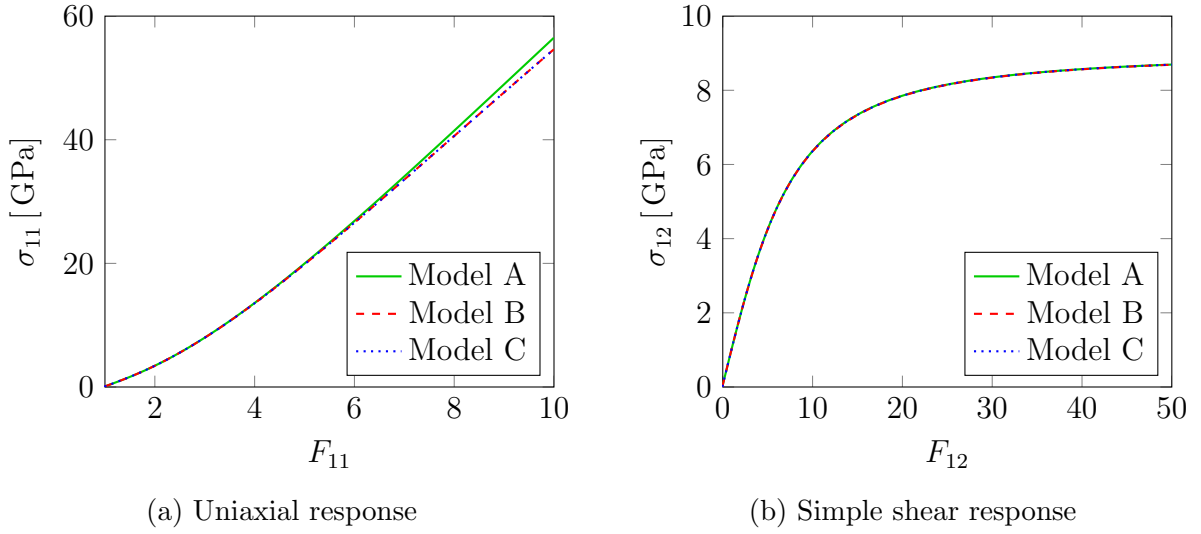
Figure 2: Numerical results

We first consider uniaxial stress in Figure 2a, by letting the normal deformation gradient F_{11} increase from 1 to 10 while keeping the Cauchy stresses $\sigma_{22} = \sigma_{33} = 0$ ($\boldsymbol{\sigma} = \boldsymbol{\tau}/I_{3\mathrm{F}}$). As previously shown theoretically, model B and C give the same response. Model A gives a somewhat stiffer response at large deformations, due to the different choice of free energy.

In the case of simple shear loading, Figure 2b shows that the response of all the models coincide. While this is expected for model B and C, the fact that model A and C coincide is explained with simple shear being an isochoric process ($I_{3\mathrm{F}} = I_{3\mathrm{F_p}} = 1 \Rightarrow I_{3\mathrm{F_e}} = 1$)

The results in Figure 2 show negligible differences between the different formulations of free energy. From a theoretical point of view, one could argue that the deviatoric dependence of the back-stress is more correct, based on the experimental evidence of volume preservation for metal plasticity.

4   ARMSTRONG-FREDERICK SATURATION

Linear kinematic hardening was considered in Section 2, for which Dettmer and Reese [4] set $\boldsymbol{F}_{\mathrm{kp}} = \boldsymbol{I}$, yielding the reduced dissipation inequality in Equation (12). If the general case with an evolving $\boldsymbol{F}_{\mathrm{kp}}$ is considered, the reduced dissipation inequality, using Equation (11), becomes

$$D = \left(\bar{\boldsymbol{M}} - {}^1\bar{\boldsymbol{M}}_{\mathrm{k}}\right) : \bar{\boldsymbol{L}}_{\mathrm{p}} + {}^1\bar{\boldsymbol{M}}_{\mathrm{k}} : \left(\boldsymbol{F}_{\mathrm{ke}}\bar{\bar{\boldsymbol{L}}}_{\mathrm{kp}}\boldsymbol{F}_{\mathrm{ke}}^{-1}\right) \tag{34}$$

From this the kinematic stress of Mandel type on the kinematic configuration ${}^1\bar{\bar{\boldsymbol{M}}}_{\mathrm{k}}$ is defined as

$$ {}^1\bar{\bar{\boldsymbol{M}}}_{\mathrm{k}} = \boldsymbol{F}_{\mathrm{ke}}^{\mathrm{t}}\, {}^1\bar{\boldsymbol{M}}_{\mathrm{k}}\boldsymbol{F}_{\mathrm{ke}}^{-\mathrm{t}} \tag{35}$$

Saturation is motivated by the rheological model, setting the evolution on $\bar{\bar{\boldsymbol{L}}}_{\mathrm{kp}}^{\mathrm{sym}}$. As the Mandel stresses in [4] are symmetric, this can be written as

$$\bar{\bar{\boldsymbol{L}}}_{\mathrm{kp}} = \dot{\lambda} \frac{^1\bar{\bar{\boldsymbol{M}}}_{\mathrm{k}}^{\mathrm{t}}}{b_\infty} \tag{36}$$

where b_∞ is a material parameter controlling the kinematic saturation. Equation (11) and (35) then yield

$$\bar{\boldsymbol{L}}_{\mathrm{ke}} = \bar{\boldsymbol{L}}_{\mathrm{p}} - \dot{\lambda} \frac{^1\bar{\boldsymbol{M}}_{\mathrm{k}}^{\mathrm{t}}}{b_\infty} \tag{37}$$

This equation can be compared with Wallin et al. [5], who use a modified potential Φ_{kin}^* to obtain

$$\bar{\boldsymbol{L}}_{\mathrm{ke}} = \dot{\lambda} \frac{\partial \Phi_{\mathrm{kin}}^*}{\partial \left(^2\bar{\boldsymbol{M}}_{\mathrm{k}}\right)} = -\bar{\boldsymbol{L}}_{\mathrm{p}} + \dot{\lambda} \frac{^2\bar{\boldsymbol{M}}_{\mathrm{k}}^{\mathrm{t}}}{b_\infty} \tag{38}$$

$\bar{\boldsymbol{L}}_{\mathrm{ke}}$ will be symmetric if a modified yield potential Φ_{kin}^* exists and we have, as before, symmetric Mandel stresses. This is the case for the considered model with Armstrong-Frederick type of non-linear kinematic saturation. $\bar{\boldsymbol{L}}_{\mathrm{ke}}$ is also symmetric in the work by Zhu et al. [11], where the first framework was extended to include nonlinear kinematic hardening of Ohno-Wang type. When $\bar{\boldsymbol{L}}_{\mathrm{ke}}$ is symmetric, the same arguments as before relating to Equations (29) and (30) hold true. Hence, for appropriate free energies the two frameworks give the same model also for nonlinear kinematic hardening.

5 CONCLUDING REMARKS

We have shown that the two different frameworks, introduced by [4] and [5], can give equivalent models for isotropic free energies. The major difference between the models used for the different frameworks is the kinematic free energy. To obtain the same model, the same structure of the kinematic free energy must be used, but with a different variable ($\bar{\bar{\boldsymbol{C}}}_{\mathrm{ke}}$ or $\bar{\boldsymbol{c}}_{\mathrm{ke}}$). The numerical results confirm these theoretical findings. They further show that the difference between the formulations of free energy has a negligible effect on the material response up to a stretch of 5 for uniaxial loading, and no effect during simple shear.

6 ACKNOWLEDGMENTS

REFERENCES

[1]   F. A. M Alwahdi, A. Kapoor, and F. J. Franklin. "Subsurface microstructural analysis and mechanical properties of pearlitic rail steels in service". In: *Wear* 302.1-2 (2013), pp. 1453–1460. DOI: 10.1016/j.wear.2012.12.058.

[2]   K. Cvetkovski and J. Ahlström. "Characterisation of plastic deformation and thermal softening of the surface layer of railway passenger wheel treads". In: *Wear* 300.1-2 (2013), pp. 200–204. DOI: 10.1016/j.wear.2013.01.094.

[3]   A. Lion. "Constitutive modelling in finite thermoviscoplasticity: a physical approach based on nonlinear rheological models". In: *International Journal of Plasticity* 16.5 (2000), pp. 469–494. DOI: 10.1016/S0749-6419(99)00038-8.

[4]   W. Dettmer and S. Reese. "On the theoretical and numerical modelling of Armstrong-Frederick kinematic hardening in the finite strain regime". In: *Computer Methods in Applied Mechanics and Engineering* 193.1 (2004), pp. 87–116. DOI: 10.1016/j.cma.2003.09.005.

[5]   M. Wallin, M. Ristinmaa, and N. S. Ottosen. "Kinematic hardening in large strain plasticity". In: *European Journal of Mechanics - A/Solids* 22.3 (2003), pp. 341–356. DOI: 10.1016/S0997-7538(03)00026-3.

[6]   M. Wallin and M. Ristinmaa. "Deformation gradient based kinematic hardening model". In: *International Journal of Plasticity* 21.10 (2005), pp. 2025–2050. DOI: 10.1016/j.ijplas.2005.01.007.

[7]   G. Johansson, J. Ahlström, and M. Ekh. "Parameter identification and modeling of large ratcheting strains in carbon steel". In: *Computers and Structures* 84.15-16 (2006), pp. 1002–1011. DOI: 10.1016/j.compstruc.2006.02.016.

[8]   N. Larijani, G. Johansson, and M. Ekh. "Hybrid micro-macromechanical modeling of anisotropy evolution in pearlitic steel". In: *European Journal of Mechanics - A/Solids* 38 (Mar. 2013), pp. 38–47. DOI: 10.1016/j.euromechsol.2012.09.011.

[9]   J. C. Simo. "A Framework For Finite Strain Based on Maximum plastic dissipation and the multiplicative decomposition: Part I. Continuum formulation". In: *Computer Methods in Applied Mechanics and Engineering* 66 (1988), pp. 199–219.

[10] I. N. Vladimirov, M. P. Pietryga, and S. Reese. "On the modelling of non-linear kinematic hardening at finite strains with application to springback - Comparison of time integration algorithms". In: *International Journal for Numerical Methods in Engineering* 75.1 (July 2008), pp. 1–28. DOI: 10.1002/nme.2234.

[11] Y. Zhu et al. "An extended cyclic plasticity model at finite deformations describing the Bauschinger effect and ratchetting behavior". In: *13th International Conference on Fracture 2013, ICF 2013* 5 (2013), pp. 1–11.

[12] J. Korelc. "Multi-language and Multi-environment Generation of Nonlinear Finite Element Codes". In: *Engineering with Computers* 18.4 (Nov. 2002), pp. 312–327. DOI: 10.1007/s003660200028.